Two-fermion–four-boson description of ^{198}Hg within the $U_\nu(6/12) \otimes U_\pi(6/4)$ extended nuclear structure supersymmetry

C. Bernards,* S. Heinze, J. Jolie, C. Fransen, A. Linnemann, and D. Radeck
Institut für Kernphysik, Universität zu Köln, Zülpicher Straße 77, D-50937 Köln, Germany
(Received 22 July 2008; revised manuscript received 23 December 2008; published 11 May 2009)

Using the $U_\nu(6/12) \otimes U_\pi(6/4)$ extended supersymmetry, we constructed the energy spectrum and electromagnetic transition properties of the supermultiplet member ^{198}Hg with two proton fermions coupled to a neutron boson core. Consistency between the supersymmetric interacting boson fermion fermion approximation (IBFFA) description and the F-spin symmetric interacting boson approximation (IBA-2) description is shown for this two-fermion–N-boson multiplet member. The data of a $\gamma\gamma$ angular correlation experiment using the HORUS cube γ-ray spectrometer—determining new multipole mixing ratios, level spins, γ transitions, and energy states—shows quite a good agreement, also for the low-energy part of the spectrum, when comparing theoretical predictions and experimental data. This is contrary to the usual assumption that a two-fermion–N-boson constellation should describe just the excited two-quasiparticle states.

DOI: 10.1103/PhysRevC.79.054307 PACS number(s): 21.60.Fw, 23.20.En, 25.55.−e, 27.80.+w

I. INTRODUCTION

Within the interacting boson approximation (IBA) [1], valence nucleon pairs are described pairwise by bosons, leading to a remarkable simplification of the description of many nuclei. Even-even nuclei with 2N valence nucleons can couple to N s ($l = 0$) and d ($l = 2$) bosons in the sd IBA and allow the description in a boson space spanned by the irreducible representation (irrep) $[N]$ of $U^B(6)$. The sd IBA has three dynamical symmetries associated with the $U(5)$, $O(6)$, and SU(3) subalgebras of U(6) [1]. The interacting boson fermion approximation (IBFA) [2] extends the N IBA bosons by an additional uncoupled fermion and allows the description of odd-A nuclei in the space spanned by the irrep $[N] \times [1]$ of $U^B(6) \otimes U^F(M)$, where M is the dimension of the single-particle space: $M = \sum_j (2j + 1)$. If the corresponding Hamiltonian exhibits a dynamical Bose-Fermi symmetry, it is analytically solvable.

In 1980, F. Iachello introduced dynamical supersymmetries in nuclei [3]. By embedding the Bose-Fermi symmetry in a graded Lie algebra $U(6/M)$, it is possible to describe an even-even nucleus with $\mathcal{N}$ bosons and an odd-A nucleus with $\mathcal{N} - 1$ bosons and a single fermion within a space spanned by the irrep $[\mathcal{N}]$. Introducing the neutron-proton degree of freedom, supersymmetry was extended so that it allows the description of an even-even, odd-neutron, odd-proton, and odd-odd nucleus in a space spanned by $[\mathcal{N}_\nu] \times [\mathcal{N}_\pi]$ [4]. Twenty years later, strong evidence for the so-called extended supersymmetry model $U_\nu(6/12) \otimes U_\pi(6/4)$ was presented in Refs. [5–7]. This model considers sd bosons and $j_\nu = 1/2, 3/2, 5/2$ and $j_\pi = 3/2$ fermions and has turned out to be applicable to the description of nuclei in the Au-Pt mass region [4–9].

When approaching single-closed shells, the description of the low-lying states of nuclei within the interacting boson approximation [1] is believed to become questionable, because the boson approximation neglects n-particle–n-hole excitations and "single-particle" effects, which are outside the model space (e.g., $L = 4$ fermion pairs, intruder states, etc.). Nevertheless, the model has been applied with quite some success to many nuclei that are only two valence nucleons (proton or neutron) away from a closed shell and can be extended to describe intruder states [10].

Within this paper it is shown how, in the framework of the extended supersymmetry $U_\nu(6/12) \otimes U_\pi(6/4)$, a description of two proton fermions coupled to N neutron bosons can be obtained to describe even-even Hg isotopes and how such an interacting boson fermion fermion approximation (IBFFA) description can be related to the IBA-2 description. So far, the supersymmetric description of that case was always believed to describe higher excited two-quasiparticle states but not the complete low-energy spectrum [2]. Referring to the results of our investigation on the nucleus ^{198}Hg, the two-fermions–four-bosons prediction seems to describe the low-energy spectrum of ^{198}Hg quite well contrary to usual assumptions. It should, however, be noted that the model uses a very truncated model space and is not considering an $s_{1/2}$ proton orbit. In Ref. [11], using the transfer reaction ^{197}Au(^{3}He,d), some $s_{1/2}$ proton transfer was observed in addition to the dominant $d_{3/2}$ proton transfer.

II. SUPERSYMMETRIC APPROACH

In the extended supersymmetric approach, multiplets of nuclei with a constant number $\mathcal{N}_\rho = N_\rho + M_\rho$ with $\rho = \nu, \pi$ of bosons and fermions are described with the same algebraic Hamiltonian. The Hamiltonian in the case of the $U_\nu(6/12) \otimes U_\pi(6/4)$ F-spin symmetric O(6) limit supersymmetry is given by [4]

$$H = a \cdot C_2\left(U^{BF}_{\nu\pi}(6)\right) + b \cdot C_2\left(O^{BF}_{\nu\pi}(6)\right) + \bar{b} \cdot C_2\left(\bar{O}^{BF}_{\nu\pi}(6)\right) + c \cdot C_2\left(O^{BF}_{\nu\pi}(5)\right) + d \cdot C_2\left(O^{BF}_{\nu\pi}(3)\right) + e \cdot C_2\left(SU^{BF}_{\nu\pi}(2)\right), \quad (1)$$

*bernards@ikp.uni-koeln.de

and has the energy eigenvalues

$$\begin{aligned} E = {} & a[N_1(N_1+5)+N_2(N_2+3)] \\ & + b[\sigma_1(\sigma_1+4)+\sigma_2(\sigma_2+2)+\sigma_3 2] \\ & + \bar{b}[\bar{\sigma}_1(\bar{\sigma}_1+4)+\bar{\sigma}_2(\bar{\sigma}_2+2)+\bar{\sigma}_3 2] \\ & + c[\tau_1(\tau_1+3)+\tau_2(\tau_2+1)] \\ & + d[L(L+1)]+e[J(J+1)]. \end{aligned} \tag{2}$$

The branching rules for the irreps of the different groups can be found in Refs. [8,12].

Up to now, one has always restricted the number of fermions of one kind to either 0 or 1 and assumed that the $M = 2$, $N = \mathcal{N} - 2$ member of the supermultiplet describes higher-lying two-quasiparticle excitations in even-even nuclei [2]. This is caused by the fact that one then treats part of the nucleons as bosons and part as fermions resembling a broken boson pair. This need not always to be the case, however, as shown in this work, since it concerns two proton fermions in the absence of proton bosons and shows direct correspondence to the interacting boson model (IBM-2), which describes low-lying states.

An interesting case for exploring the two-fermion member of the supermultiplet can be found within the O(6) limit of the $\mathrm{U}_\nu(6/12) \otimes \mathrm{U}_\pi(6/4)$ supersymmetry, which has already been successfully applied to several nuclei in the Au-Pt mass region, i.e., the quartet ^{196}Pt, ^{197}Au, ^{197}Pt, and ^{198}Au [4]. In this extended supersymmetry, the reduction rule applies to the neutrons and protons separately: $\mathcal{N}_\nu = N_\nu + M_\nu$ and $\mathcal{N}_\pi = N_\pi + M_\pi$. In application to the quartet around ^{196}Pt, $[\mathcal{N}_\nu] \times [\mathcal{N}_\pi\}$ is equal to $[4\} \times [2\}$. For $\mathcal{N}_\nu = 4$, the requirement $\mathcal{N}_\pi = 2$ can be fulfilled for three different nuclei: the usual even-even nucleus ^{196}Pt ($N_\pi = 2$, $M_\pi = 0$) and the odd-even nucleus ^{197}Au ($N_\pi = 1$, $M_\pi = 1$), but also one has the case of two $j_\pi = 3/2$ fermions coupled to a neutron boson core ($N_\pi = 0$, $M_\pi = 2$) which should describe ^{198}Hg [13]. Note that in this case, all protons or neutrons get treated as the same kind of particle (boson or fermion).

III. CONSISTENCY OF THE IBFFA AND IBA-2 DESCRIPTION

From now on we focus on the two-fermions–four-bosons nucleus ^{198}Hg, construct the level scheme, deduce the $M1$ tensor character, and compare the IBFFA description with the pure bosonic IBA-2 description. Because just proton fermions coupled to a bosonic neutron core are considered, the $\mathrm{U}_\nu(6/12) \otimes \mathrm{U}_\pi(6/4)$ group chain given in Ref. [4] reduces to

$$\begin{array}{ccccccccc} \mathrm{U}(6/4) & \supset & \mathrm{U}^B(6) \otimes \mathrm{U}^F(4) & \supset & \mathrm{O}^B(6) \otimes \mathrm{SU}^F(4) & \supset & \mathrm{O}^{BF}(6) & \supset \mathrm{O}^{BF}(5) & \supset \mathrm{SU}^{BF}(2). \\ \downarrow & & \downarrow \quad \downarrow & & \downarrow \quad \downarrow & & \downarrow & \downarrow & \downarrow \\ [\mathcal{N}\} & & [N_b] \quad [1,1] & & (\Sigma_b) \quad [1,1] & & \langle\sigma_1,\sigma_2,\sigma_3\rangle & (\tau_1,\tau_2) & J \end{array} \tag{3}$$

The new reduction rules of the $[N] \times [0] \times [0] \times [1,1]$ representation of $U_\nu^B(6) \otimes \mathrm{U}_\nu^F(12) \otimes \mathrm{U}_\pi^B(6) \otimes \mathrm{U}_\pi^F(4)$ is $\langle\Sigma_b\rangle \times [1,1]$ giving $\langle\Sigma_b+1,0,0\rangle$, $\langle\Sigma_b,1,0\rangle$, and $\langle\Sigma_b-1,0,0\rangle$. All other reduction rules can be found in Refs. [8,12].

Now, the Hamiltonian (1) can be rewritten as

$$\begin{aligned} H = {} & D \cdot C_2(\mathrm{O}^B(6)) + A \cdot C_2(\mathrm{SO}^{BF}(6)) \\ & + B \cdot C_2(\mathrm{O}^{BF}(5)) + C \cdot C_2(\mathrm{SU}^{BF}(2)) \end{aligned} \tag{4}$$

up to a constant contribution. The energy eigenvalues are

$$\begin{aligned} E = {} & D[\Sigma_b(\Sigma_b+4)] \\ & + A[\sigma_1(\sigma_1+4)+\sigma_2(\sigma_2+2)+\sigma 2_3] \\ & + B[\tau_1(\tau_1+3)+\tau_2(\tau_2+1)] + C[J(J+1)]. \end{aligned} \tag{5}$$

The relation between the parameters in Hamiltonians (1) and (4) is given by

$$A = \bar{b}, \quad B = c, \quad C = d + e. \tag{6}$$

The parameter D has no equivalent in Eq. (1).

In Fig. 1, the resulting level scheme for energy equation (5) is shown using parameters obtained by a least-squares fit to the ^{196}Pt quartet [4,13] with $A = -0.097$, $B = 0.042$, and $C = 0.025$. The parameters are given in MeV. All states in Fig. 1 are marked with their quantum numbers $\langle\sigma_1,\sigma_2,\sigma_3\rangle$, (τ_1,τ_2), and spin J. Since only the low-energy states with $\Sigma_b = 4$ are of interest, the last parameter was fixed to $D = -100$ to shift states with $\Sigma_b = 0$ or 2 to higher energies. A comparison with the experimental ^{198}Hg data available in 1986 is given in Ref. [13]. It shows quite a good matching and strongly encourages further experimental tests.

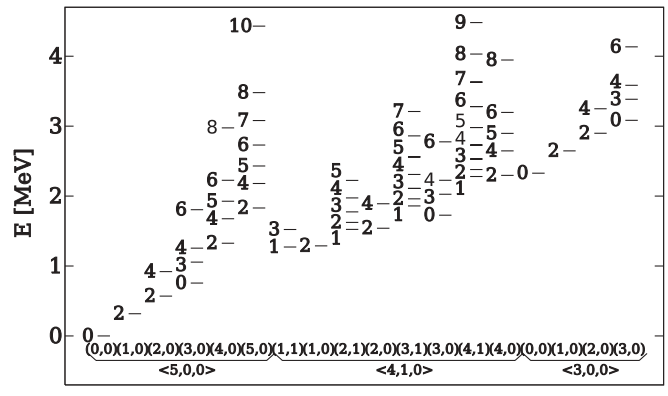

FIG. 1. Resulting spectrum for two proton fermions coupled to an $N = 4$ neutron core using energy equation (5) and parameters of the ^{196}Pt quartet [4]. Also given are the quantum numbers of the states which are all of positive parity.

The description of ^{198}Hg can also be done within the IBA-2 model. By replacing the proton holes by an sd boson, one can describe the nucleus ^{198}Hg using the F-spin symmetric O(6) limit of the IBA-2. The corresponding group chain with its labels, Hamiltonian, and energy eigenstates are given by [14]

$$\begin{array}{ccccccc} \mathrm{U}_\nu(6) & \otimes & \mathrm{U}_\pi(6) & \supset & \mathrm{U}_{\nu\pi}(6) & \supset & \\ \downarrow & & \downarrow & & \downarrow & & \\ [N_\nu] & & [N_\pi] & & [N-f,N] & & \\ \mathrm{O}_{\nu\pi}(6) & \supset & \mathrm{O}_{\nu\pi}(5) & \supset & \mathrm{O}_{\nu\pi}(3) & & \\ \downarrow & & \downarrow & & \downarrow & & \\ \langle\sigma_1,\sigma_2,0\rangle & & (\tau_1,\tau_2) & & J & & \end{array}, \tag{7}$$

$$H = D'\cdot C_2(\mathrm{U}_{\nu\pi}(6)) + A\cdot C_2(\mathrm{O}_{\nu\pi}(6)) + B\cdot C_2(\mathrm{O}_{\nu\pi}(5)) + C\cdot C_2(\mathrm{O}_{\nu\pi}(3)), \tag{8}$$

and

$$E = D'[(N-f)(N-f+5)+f(f+3)] + A[\sigma_1(\sigma_1+4)+\sigma_2(\sigma_2+2)] + B[\tau_1(\tau_1+3)+\tau_2(\tau_2+1)] + C[J(J+1)]. \tag{9}$$

By using the reduction rules, it can be shown that the representation $[4]\times[1,1]$ of the $U^B(6)\otimes \mathrm{U}^F(4)$ algebra contains exactly the same O(6) representations as the $[4]\times[1]$ representation of the $U_\nu(6)\otimes \mathrm{U}_\pi(6)$ algebra. Neglecting the parameters D and D', we note that Eq. (9) is equal to energy equation (5) and produces the same level scheme for the IBA-2, Eq. (7), and the IBFFA group chain, Eq. (3). Note that when two neutron fermions couple to N proton bosons, different results arise.

Another more intuitive view is to look at the possible resulting spins of two coupled $j = 3/2$ fermions. They can couple only to $J = 0$ and $J = 2$, yielding exactly the intrinsic spins of the bosons in the sd IBA-2 description.

The relation of both descriptions can also be shown for the $M1$ transitions. The $M1$ operator is given by a linear combination of the generators of the $U^B(6)\otimes \mathrm{U}^F(4)$ algebra which couple to $J = 1$ by

$$\hat{T}^{M1} = \alpha[d^\dagger\times\tilde{d}]^{(1)} + \beta[a^\dagger_{3/2}\times\tilde{a}_{3/2}]^{(1)}. \tag{10}$$

The matrix elements of both terms of the $M1$ operator are connected by the simple relationship [2]

$$\langle\psi_1\|[d^\dagger\times\tilde{d}]^{(1)}_m\|\psi_2\rangle = -\frac{1}{\sqrt{2}}\langle\psi_1\|[a^\dagger_{3/2}\times\tilde{a}_{3/2}]^{(1)}_m\|\psi_2\rangle. \tag{11}$$

Thanks to relation (11), it is sufficient to treat just one kind of particle: bosons or fermions. The tensor character of the bosonic creation and annihilation operators is given by

$$\begin{aligned} d^\dagger_m &\mathrel{\widehat{=}} T^{[1]\times[0],(1)\times[0],\langle1\rangle,(1),2,m},\\ \tilde{d}_m &\mathrel{\widehat{=}} T^{[15]\times[0],(1)\times[0],\langle1\rangle,(1),2,m}. \end{aligned} \tag{12}$$

By calculating the outer product, respecting the corresponding groups, and using the branching rules, one gets the tensor character of the coupled bosonic operator as

$$[d^\dagger\times\tilde{d}]^{(1)} \mathrel{\widehat{=}} T^{[2,14]\times[0],(1,1)\times[0],\langle1,1\rangle,(1,1),1,m}, \tag{13}$$

which leads to the following selection rules for $M1$ transitions [15]:

$$\Delta\sigma_1 \leqslant 1 \wedge \Delta\sigma_2 \leqslant 1 \wedge \Delta\tau_1 = \Delta\tau_2 \leqslant 1. \tag{14}$$

An example of an analytical solution for the matrix element is

$$|\langle\langle 4,1,0\rangle(1,1)1\|[d^\dagger\times\tilde{d}]^{(1)}\|\langle 5,0,0\rangle(2,0)2\rangle|^2 = \frac{3(N_b+5)(N_b+6)}{20(N_b+1)(N_b+2)}. \tag{15}$$

Squares of the absolute values of the reduced matrix elements of the $M1$ operator for transitions between eigenstates of the Hamiltonian (4) can also be calculated numerically with the computer code ARBMODEL [15]. The result of Eq. (15) for $N_b = 4$ is 9/20 and is identical to the calculated value of the ARBMODEL calculation.

The corresponding analytical solution for the sd IBA-2 is given in Ref. [14]. Since two fermions are now treated as one boson, one has to substitute the number of particles. In IBA-2 for the O(6) limit, the following $B(M1)$ value is obtained:

$$B(M1;1^+_M\to 2^+_2) = \frac{3}{4\pi}(g_\nu-g_\pi)2\frac{(N+4)(N+5)}{2(N-1)N(N+1)}N_\nu N_\pi. \tag{16}$$

To compare the reduced matrix element of $[d^\dagger\times\tilde{d}]^{(1)}$ within the Bose-Fermi symmetry, one has to set $g_\pi = 1$ and $g_\nu = 0$. Respecting the prefactor of the $M1$ operator in Ref. [14],

$$T(M1) = \sqrt{\frac{30}{4\pi}}\cdot[g_\nu(d^\dagger_\nu\times\tilde{d}_\nu)^{(1)} + g_\pi(d^\dagger_\pi\times\tilde{d}_\pi)^{(1)}], \tag{17}$$

and a factor of 3 given by the conversion of the $B(M1)$ to the reduced matrix element, a factor of $4\pi/10$ is obtained. With the substitution $N\to N_b+1$, $N_\pi\to 1$, and $N_\nu\to N_b$, Eq. (16) results in Eq. (15). The agreement of both descriptions can be successfully confirmed for other electromagnetic transitions as well.

In addition, other observables can be calculated. An important one is the one-proton transfer strengths from ^{197}Au to ^{198}Hg. Like in $U(6/4)$, the transfer operator is taken as proportional to the $\tilde{a}_{3/2}$ operator, leading to the important selection rules [2]

$$\Delta|\sigma_1| = \Delta|\tau_1| = \tfrac{1}{2}. \tag{18}$$

These rules only allow transfer to the ground state and the lowest 2^+ state in ^{198}Hg, with a ratio equal to $(\mathcal{N}-1)/(\mathcal{N}+3)$. In Ref. [11], using the transfer reaction ^{197}Au(^{3}He,d), dominant $d_{3/2}$ proton transfer to the ground state was observed, but the strength to the excited states was found to be fragmented over several 2^+ states in strong contradiction to the O(5) selection rule of Eq. (18). It was concluded that the transfer operator is too simple and does not allow core excitations. As noted in Ref. [2], this failure is also observed for transfer between ^{193}Ir and ^{194}Pt. Also important is that $s_{1/2}$ and $d_{5/2}$ proton transfer to the first 2^+ and 4^+ states was observed in addition to the dominant $d_{3/2}$ proton transfer to the 0^+ and 2^+ states. This indicates that our model space is too restricted to describe all experimental observables in detail.

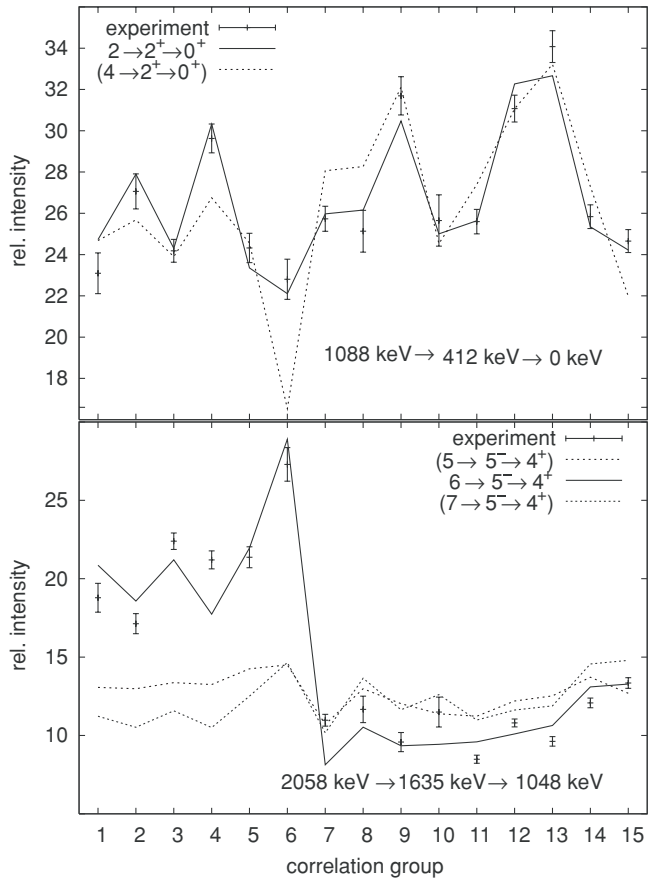

FIG. 2. Top: $\gamma\gamma$ angular correlation plot using 15 different correlation groups showing the $2_2^+ \rightarrow 2_1^+ \rightarrow 0_1^+$ decay cascade fit with $\delta(2^+ \rightarrow 2^+) = 0.95^{+0.23}_{-0.19}$ in comparison with a hypothetical $4 \rightarrow 2 \rightarrow 0$ cascade. Bottom: Plot for spin determination of a possible $J = 5, 6$, or 7 state with $\delta(6^- \rightarrow 5^-) = -1.78(23)$.

IV. EXPERIMENT

To obtain experimental data on ^{198}Hg, an experiment was performed at the Tandem accelerator at the Institute for Nuclear Physics of the University of Cologne. Using a ^{4}He beam with an energy of 25 MeV impinging a 10 mg/cm^2 ^{196}Pt target, the reaction ^{196}Pt$(\alpha,2n)^{198}$Hg was induced. To analyze the γ decays of the excited yrast and nonyrast ^{198}Hg states, eight single high-purity germanium detectors and a seven-fold segmented germanium cluster array mounted on the HORUS cube γ-ray spectrometer were used.

The cube-like setup of the HORUS spectrometer allows the analysis of $\gamma\gamma$ angular correlations, which can be used to determine level spins and multipole mixing ratios of γ transitions. Coincidentally detected γ rays are sorted and summed up into 15 different correlation group matrices, depending on the geometry of the associated detectors. This technique is explained in detail in, for instance, Ref. [16]. Typical $\gamma\gamma$ angular correlation plots are shown in Fig. 2. The angular correlation analysis is done with the code CORLEONE [17], which fits angular distributions for correlated γ quanta as described in Refs. [18,19] to the experimentally measured intensities in the different correlation groups. In this way, level spins and multipole mixing ratios can be determined. In combination with γ selection rules, the determined multipole mixing ratio δ allows parity assignment in some cases. In total, 1.2×10^9 $\gamma\gamma$ coincidences were used to construct the low-energy level scheme of ^{198}Hg up to an excitation energy of 2.4 MeV. Figure 3 shows coincidence spectra to the $2_1^+ \rightarrow 0_1^+$ transition up to an energy of 1600 keV.

In the following we discuss some levels that were investigated. The complete results in comparison with the present NNDC data [20] can be found in Table I.

1087.5 keV, 2^+. In agreement with formerly published data [20], the multipole mixing ratio could be determined with $\delta(2^+ \rightarrow 2^+) = +0.95^{+0.23}_{-0.19}$. A corresponding plot for a spin 2 hypothesis in comparison with a spin 4 hypothesis is shown in Fig. 2. The determined branching ratio matches the published data [20].

1401.6 keV, 0^+. Investigating the $E_\gamma = 990.0$ keV decay to the 2_1^+ state at $E = 411.6$ keV, a doublet was found showing coincidence with the yrast state decays up to the 6_1^+ state at $E = 1815.5$ keV. The existence of the $0_2^+ \rightarrow 2_1^+$ transition [20] could be confirmed by analyzing the intensities of the $2_1^+ \rightarrow 0_1^+$ decay in different coincidence spectra, gating on the 990.0 keV γ transitions and gating on the 767.3 keV $6_1^+ \rightarrow 4_1^+$ decay. In coincidence to the new 990 keV doublet in coincidence to the $6_1^+ \rightarrow 4_1^+$ decay another formerly not observed γ transition with $E_\gamma = 774$ keV was found.

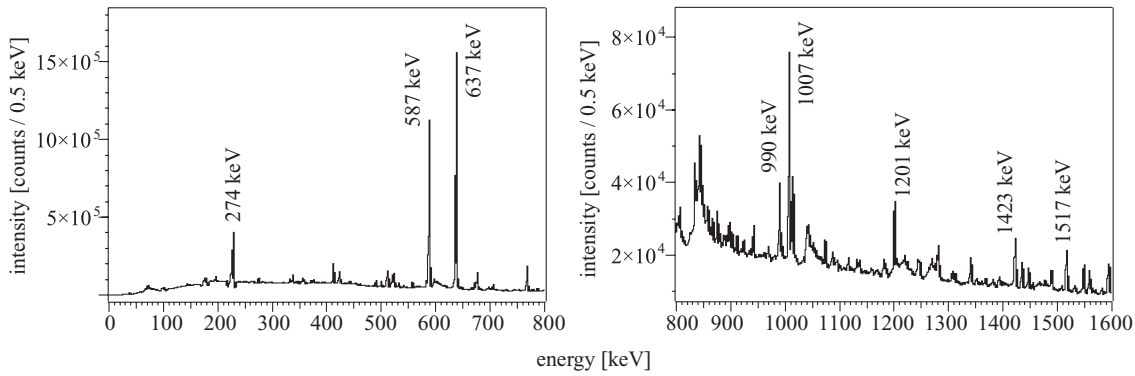

FIG. 3. Spectra up to 1600 keV in coincidence to the $2_1^+ \rightarrow 0_1^+$ transition at $E_\gamma = 411.6$ keV. The most intensive peaks are labeled with their associated γ energy.

TABLE I. Data of this experiment compared with data of the National Nuclear Data Center [20]. Level energies E_{Level} and decays E_γ printed in *italic* could not be observed or confirmed. Energies and spins labeled with an * are new or differ from NNDC data.

E_{Level} (keV)	J^π	E_γ (keV)	Branching ratio	Branching ratio [20]	δ	δ [20]		E_{Final} (keV)	J^π
0.0	0^+								
411.6 2	2^+	411.6 2	100	100			$E2$	0.0	0^+
1048.2 3	4^+	636.5 2	100	100			$E2$	411.6	2^+
1087.5 3	2^+	675.7 2	100 (10)	100.0 (4)	$+0.95^{+0.23}_{-0.19}$	+1.07 (14)	$M1+E2$	411.6	2^+
		1087.5 2	20 (4)	19.8 (3)			$E2$	0.0	0^+
1401.6 4	0^+	990.0 4		100			$E2$	411.6	2^+
		1401.7 8					$E0$	0.0	0^+
1419.0 3	3^{+*}	331.5 2	26 (6)	21 (4)				1087.5	2^+
		370.7 2	10 (2)	11 (2)				1048.2	4^+
		1007.4 2	100 (10)	100 (10)	$+1.10^{+0.52}_{-0.34}$		$M1+E2$	411.6	2^+
1548.4 4	$(1, 2^+)$	1136.8 2		100 (9)				411.6	2^+
		1548.4 3		29 (6)				0.0	0^+
1550	0^+								
1612.2 3	2^+	564.0 3		3.1 (6)				1048.2	4^+
		1200.5 2		100 (10)	−0.25(14)	−0.26(5)	$M1+E2$	411.6	2^+
		1611.8 8		9.9 (5)				0.0	0^+
1635.3 3	5^-	587.1 2	100	100	−0.04(3)		$E1$	1048.2	4^+
1683.3 3	7^-	*47.74 5*		100			$E2$	1635.3	5^-
1760 15	0^+								
1815.5 3	6^+	767.3 2	100	100	+0.01(5)		$E2$	1048.2	4^+
1832.1 4	2^+	*745.0 8*		1.6 (7)				1087.5	2^+
		1420.5 4		100 (11)		−0.18(3)	$M1(+E2)$	411.6	2^+
		1832.1 4		53 (6)				0.0	0^+
1834.6 4	4^+	747.2 4	32 (6)	27 (16)	−0.07(10)		$E2$	1087.5	2^+
		786.2 4	68 (14)	100 (16)	−0.39(23)		$M1+E2$	1048.2	4^+
		1423.0 2*	100 (10)					411.6	2^+
1846.8 4	3^{+*}	234.6 2		12.8 (19)				1612.2	2^+
		759.4 2		42 (4)	−0.56(16)		$M1+E2$	1087 5	2^+
		789.8 2		31 (2)				1048.2	4^+
		1435.1 2		100 (13)	+0.00(11)	+0.15(5)	$M1(+E2)$	411.6	2^+
1858.7 7	2^+	771.0 8		3.6 (5)				1087.5	2+
		810.4 4		4.1 (8)				1048.2	4^+
		1447.1 2		100 (11)		−0.20(5)	$M1(+E2)$	411.6	2^+
		1859 1		18 (3)				0.0	0^+
1899.0 6	$1^+, 2^+$	498.0 4		10 (1)				1401.6	0^+
		1486.5 8		15 (7)				411.6	2^+
		1899.0 4		100 (10)				0.0	0^+
1901.1 6	(2^+)	*853.0 4*		5.4 (14)				1048.2	4^+
		1489.5 4	100	100 (12)		−0.23(8)	$(M1+E2)$	411.6	2^+
1909.5 4	6^-	225.8 4	100 (10)	100 (15)		$+0.50^{+0.29}_{-0.03}$	$M1(+E2)$	1683.3	7^-
		273.9 2	22 (5)	28 (6)	$-0.88^{+0.31}_{-0.45}$		$M1+E2$	1635.3	5^-
1910.5 6	9^-	227.2 4	100	100			$E2$	1683.3	7^-
1928.4 4	3^-	1516.8 2*	100					411.6	2^+
1959.7 4*	$0^+, 1, 2, 3, 4^{+*}$	1548.1 2*	100					411.6	2^+
1965 6									
1970.2 4	$(2^+, 3, 4^+)$	883.0 4		10 (5)				1087.5	2^+
		922.6 4		21 (3)				1048.2	4^+
		1558.6 2		100 (11)				411.6	2^+
2005.6 10	$0^+, 1, 2, 3, 4^+$	1594 1	100	100				411.6	2^+
2048.0 4	$0^+, 1, 2, 3, 4^+$	1636.4 2	100	100				411.6	2^+
2049 6									
2058.9 4	6^{-*}	149.2 2		14 (5)				1909.5	6^-
		375.4 2		71 (15)				1683.3	7^-
		423.3 2		100 (15)	−1.78(23)		$M1+E2$	1635.3	5^-
2070.3 4	$1^+, 2^+$	1658.7 4	100	100				411.6	2^+

TABLE I. *(Continued.)*

E_{Level} (keV)	J^π	E_γ (keV)	Branching ratio	Branching ratio [20]	δ	δ [20]		E_{Final} (keV)	J^π
2090 1*	$4^+, 5^{+*}$	274.7 4*						1815.5	6^+
		671.3 2*						1419.0	3^+
		1042.6 4*						1048.2	4^+
2109.5 8	$(1, 2^+)$	1697.4 4		100 (15)				411.6	2^+
		2110.0 8		45 (12)				0.0	0^+
2125.0 4	$6^-, 7^-$	215.5 2	19 (4)	28(5)		$+0.42^{+0.30}_{-0.04}$	$M1(+E2)$	1909.5	6^-
		441.6 2	54 (11)	49 (7)			$M1$	1683.3	7^-
		489.5 2	100 (10)	100 (11)				1635.3	5^-
2132.2 6	$1, 2^+$	1044.7 8		8 (3)				1087.5	2^+
		1720.6 4		100 (10)				411.6	2^+
2135.0 6	5^-	452.2 2*						1683.3	7^-
		499.1 2*						1635.3	5^-
2169.2 8	(2^+)	*336.5 4*		17 (8)				1832.1	2^+
		621.0 5		17 (8)				1548.4	$(1, 2^+)$
		1121.1 4		<32				1048.2	4^+
		1757.6 8		100 (15)				411.6	2^+
		2168.7 5		34 (5)				0.0	0^+
2177.1 6	$(1, 2^+)$	*318.9 4*		<6				1858.7	2^+
		758.0 2		40 (10)				1419.0	3^+
		1089.8 4		67 (26)				1087.5	2^+
		1765.5 8		100 (10)				411.6	2^+
		2177.7 8		5.6 (22)				0.0	0^+
2202.2 4	$6^-, 7^-$	292.7 2		5.9 (22)				1909.5	6^-
		519.1 2		100 (12)			$M1$	1683.3	7^-
		567.0 4		5.9 (22)				1635.3	5^-
2208.6 4	$(1, 2^+)$	*238.3 2*		25 (6)				1970.2	$(2^+, 3, 4^+)$
		350.6 4		<8				1858.7	2^+
		376.8 5		20 (5)				1832.1	2^+
		596.5 4		100 (11)				1612.2	2^+
		789.6 4		49 (6)				1419.0	3^+
		1121.1 4		1.25 (25)				1087.5	2^+
		1796.8 8		50 (7)				411.6	2^+
		2209.2 4		41 (5)				0.0	0^+
2219.2 3	$0^+, 1, 2, 3, 4^+$	1131.7 2	100	100				1087.5	2^+
2267.2 4	(2^+)	1219.0 4		100 (9)				1048.2	4^+
		1855.4 8		44 (10)				411.6	2^+
		2267.0 15		2.6 (10)				0.0	0^+
2277 1*	$1^+, 2, 3, 4, 5^{+*}$	857.8 2*	100					1419.0	3^+
2286.6 8	$(1, 2^+)$	1875.0 8	100	100 (10)				411.6	2^+
		2287.5 10		66 (18)				0.0	0^+
2295.3 4	$2^+, 3, 4, 5, 6^+$	*325.0 4*		<21				1970.2	$(2^+, 3, 4^+)$
		436.9 8		45 (11)				1858.7	2^+
		448.6 4		29 (11)				1846.8	3^+
		461.0 2*						1834.6	4^+
		876.4 4		66 (8)				1419.0	3^+
		1207.8 2		100 (24)				1087.5	2^+
		1884.5 10		13 (5)				411.6	2^+
2319.8 6	$1, 2^+$	1232.3 4		100 16				1087.5	2^+
		1908.5 4		68 (11)				411.6	2^+
		2319.5 8		<74				0.0	0^+
2331.0 6	4^+	911.6 4		28 (11)				1419.0	3^+
		1243.8 2		100 (14)				1087.5	2^+
2337.0 4	8^+	521.5 2	100	100		+0.01(6)	$E2$	1815.5	6^+
2360.0 10	3^+	514.0 8		5.5 (12)				1846.8	3^+
		525.9 3		6.9 (9)				1834.6 3	4^+
		940.7 8		13.1 (12)				1419.0	3^+
		1273.5 8		7.6 (9)				1087.5	2^+

TABLE I. *(Continued.)*

E_{Level} (keV)	J^π	E_γ (keV)	Branching ratio	Branching ratio [20]	δ	δ [20]		E_{Final} (keV)	J^π
		1312.0 4		100 (11)		−0.09(3)	$M1(+E2)$	1048.2	4^+
		1949.1 5		2.5 (4)		−0.185(35)	$(M1+E2)$	411.6	2^+
2400 4									
2515.6 4	$4^-, 5, 6, 7, 8^-$	390.2 4		100 (13)				2125.2	$6^-, 7^-$
		456.74*		16 (7)				2058.9	6^-
		606.0 10		16 (7)				1909.5	6^-
		832.9 4		27 (5)				1683.3	7^-
2535.1 4	3^-	1447.6 2*	100					1087 5	2^+
2656 1*	$1^-, 2, 3, 4, 5^{-*}$	727.3 2*	100					1928.4	3^-

1419.0 keV, 3^+. The adopted spin for this level is $(2)^+$ [20]. According to our data, $J^\pi = 3^+$ can be assigned. The analysis of the most intense decay with 1007.4 keV to the 2_1^+ favors the spin hypothesis $J = 3$, whereas $J = 2$ is unlikely. The decay with 370.7 keV to the 4_1^+ is investigated in Fig. 4. The $\delta = 0$ pure $E2$ transition in the case of the $J = 2$ hypothesis can be ruled out in comparison to the $3 \to 4_1^+ \to 2_1^+$ cascade fit. In addition, we have yet-unpublished data of a β-decay experiment confirming the $J = 3$ assignment [21]. Thus, this state is identified as the 3_1^+ state in ^{198}Hg. The angular correlation of the third depopulating decay with 331.5 keV could not be analyzed due to low statistics. For the $E_\gamma = 1007.4$ keV transition, the multipole mixing ratio δ was first determined to be $\delta(3^+ \to 2^+) = +1.10^{+0.52}_{-0.34}$. For the 3_1^+ state, the branching ratios of the depopulating γ transitions were determined and found to match the already published data [20].

1548.4 keV, 1, 2^+. The adopted ground state transition with $E_\gamma = 1548.4$ keV [20] was not observed, but a γ transition at $E_\gamma = 1548.1$ keV was found in coincidence spectra of the $2_1^+ \to 0_1^+$ transition, yielding a new level at $E = 1959.7$ keV. The existence of the published 1548.4 keV ground state transition could not be confirmed.

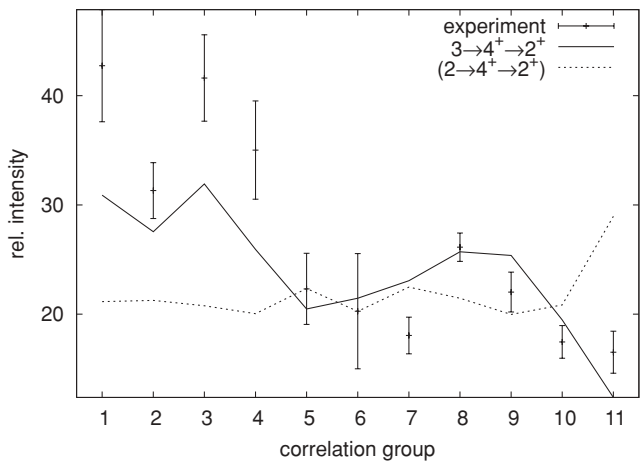

FIG. 4. Investigation of the 1419 → 1048 → 412 keV cascade by comparing a $J = 3$ and a $J = 2$ hypothesis. Although the statistics are too low to use all 15 correlation groups, the $J = 2$ hypothesis can still be ruled out.

1612.2 keV, 2^+. The published multipole mixing ratio for the $E_\gamma = 1200.5$ keV decay [20] was confirmed with $\delta(2^+ \to 2^+) = -0.25(14)$.

1635.3 keV, 5^-. For the transition $5_1^- \to 4_1^+$ with $E_\gamma = 587.1$ keV, the newly measured multipole mixing ratio $\delta(5^- \to 4^+) = -0.04(2)$ confirmed the 5^- spin assignment.

1834.6 keV, 4^+. For this state, a new γ decay with $E_\gamma = 1423.0$ keV to the 2_1^+ state was found. Two new multipole mixing ratios for the depopulating transitions were determined with $\delta(4^+ \to 2^+) = -0.07(10)$ for the 747.2 keV decay and $\delta(4^+ \to 4^+) = -0.39(23)$ for the 786.2 keV decay. The derived branching ratio matches the formerly published data with their rather large errors. The energy of the newly found γ transition is quite close to the energy of the depopulating 1420.5 keV transition of the 2^+ state at $E = 1832.1$ keV to the 2_1^+, which might be the reason why this decay was not identified in previous experiments [20].

1846.8 keV, 3^+. This state was known as $J^\pi = (3)^+$ [20]. We confirm this spin assignment. Multipole mixing ratios were determined for two depopulating transitions: the value for the most intensive γ decay with $E_\gamma = 1435.1$ keV is $\delta(3^+ \to 2^+) = +0.00(11)$, being in agreement with a formerly determined δ value [20]. The newly measured δ for the $E_\gamma = 759.4$ keV transition is $\delta(3^+ \to 2^+) = -0.56(16)$ and gives a hint for positive parity.

1909.5 keV, 6^-. For the $E_\gamma = 273.9$ keV $6^- \to 5^-$ decay, a new multipole mixing ratio was determined with $\delta(6^- \to 5^-) = -0.88^{+0.31}_{-0.45}$. In addition, a new γ transition close in energy at $E_\gamma = 274.7$ keV was found depopulating the newly found level at $E = 2090$ keV. The branching ratio was determined and matches the data of former experiments [20].

1928.4 keV, 3^-. In coincidence spectra of the $2_1^+ \to 0_1^+$ ground state transition, a new γ transition was determined with $E_\gamma = 1516.8$ keV.

2005.6 keV, $0^+, 1, 2, 3, 4^+$. The $E_\gamma = 1594$ keV decay to the 2_1^+ state appears broadened in the coincidence spectra, thus hinting for another unknown γ transition of similar energy.

2058.9 keV, 6^-. The adopted spin $(5^-, 6, 7^-)$ was firmly assigned as $J^\pi = 6^-$. In Fig. 2, a comparison of different spin hypotheses is shown using fits of a $5 \to 5^- \to 4^+$, a $6 \to 5^- \to 4^+$, and a $7 \to 5^- \to 4^+$ cascade. The hereby first determined multipole mixing ratio of the $E_\gamma = 423.3$ keV

transition to the 5_1^- is $\delta(6^- \to 5^-) = -1.78(23)$. Thus, negative parity can be assigned because of the electromagnetic selection rules and a δ strongly differing from $\delta = 0$.

2090 keV, $4^+, 5^+$. A new level was found at $E = 2090$ keV with three depopulating γ decays of $E_\gamma = 274.7, 671.3$ and 1042.6 keV to the $6_1^+, 3_1^+$, and 4_1^+ states. Possible spin assignments for that level are 4^+ and 5^+. The decay with $E_\gamma = 671.3$ keV turned out to be a doublet; a γ transition of this energy can be also found in coincidence spectra of the 587.1 keV decay of the 5_1^- state at $E = 1635.3$ keV.

2125.0 keV, $6^-, 7^-$. A doublet to the $E_\gamma = 489.5$ keV decay was found in the coincidence spectra of the depopulating transitions of the 4^+ state at $E = 1834.6$ keV. Nevertheless, the branching ratio could be determined, matching the formerly published data [20] with respect to the errors.

2135.0 keV, 5^-. Two new depopulating γ transitions were identified for the known 5^- state at $E = 2135.0$ keV: a γ decay into the 7^- state at $E = 1683.3$ keV and a transition into the 5^- state at $E = 1635.3$ keV.

2277 keV, $1^+, 2, 3, 4, 5^+$. In coincidence spectra, a new γ transition at $E_\gamma = 857.8$ keV was found and was assigned to a new state at $E = 2277$ keV decaying into the 3^+ state at 1419.0 keV.

2656 keV, $1^-, 2, 3, 4, 5^-$. A new state was determined at 2656 keV with a new γ transition at $E_\gamma = 727.3$ keV to the 3^- state at 1928.4 keV.

V. SUPERSYMMETRIC PREDICTIONS AND THE EXPERIMENTAL ^{198}Hg DATA

The predicted level scheme for ^{198}Hg in Fig. 1 is based on the parameters A, B, and C gained by fitting Eq. (5) to experimental data of the "magical quartet" around ^{196}Pt [13]. So far, no experimental data of ^{198}Hg were taken into account.

Comparison of the experimental ^{198}Hg data with the theoretical predictions of Fig. 1 shows matching in qualitative aspects, but also differences that cannot be neglected: e.g., the $J(J+1)$ splitting is too wide. This can be related to the closeness of the proton shell closure at $Z = 82$. The mismatch can be reduced by a new set of parameters.

To fit the experimental level scheme of ^{198}Hg, ten experimental levels were assigned to their supersymmetric counterparts. The assignments are based on two different criteria. First, the fitted parameters A to C and therewith the energy spectrum described by Eq. (5) should be in good agreement with the experimentally determined level energies. Additionally, the observed γ transitions were investigated for possible sets of level assignments. After determining multipole mixing ratios δ, relative $B(M1)$ and $B(E2)$ transition strengths of the γ transitions can be used to test level assignments. $M1$ fractions were tested with the derived $M1$ selection rules, Eq. (14); for the $E2$ fractions, the computer codes ARBMODEL [15] and TRANSNUCLEAR [22] were used by comparing numerically calculated $B(E2)$ values

$$B(E2; J_i \to J_f) = \frac{1}{2J_i + 1} |\langle \| T(E2) \| \rangle|2 \qquad (19)$$

with the observed $E2$ fractions. The $T(E2)$ operator is

$$T(E2) = e[(s^\dagger \times \tilde{d})^{(2)} + (d^\dagger \times \tilde{s})^{(2)} + \chi(d^\dagger \times \tilde{d})^{(2)}], \qquad (20)$$

with an effective boson charge $e = 0.18\ e$ b, and the usual O(6) value of $\chi = 0$. $e = 0.18\ e$ b is close to the effective boson charge of $|e| = 0.16\ e$ b for ^{196}Pt given in Ref. [23] and is the result of a fit to the experimentally available $B(E2; 2_1^+ \to 0_1^+)$ value. The calculated $B(E2)$ transition strengths are listed in Table III in comparison with the experimental data available [20]. In this way, different possible level assignments were tested.

Figure 5 shows the investigation of the $M1$ fraction of the γ transitions for the chosen level assignment. The investigated transitions are listed in Table II in combination with their relative $B(M1)/B(E2)$ ratios. Depending on the $B(M1)/B(E2)$ ratio and the $M1$ selection rules, the transitions are classified in three different groups marked by different arrow types as explained in the legend in Fig. 5. Because the level lifetimes are unknown, it is not possible to calculate absolute transition strength. The γ transitions with an $M1$ fraction do

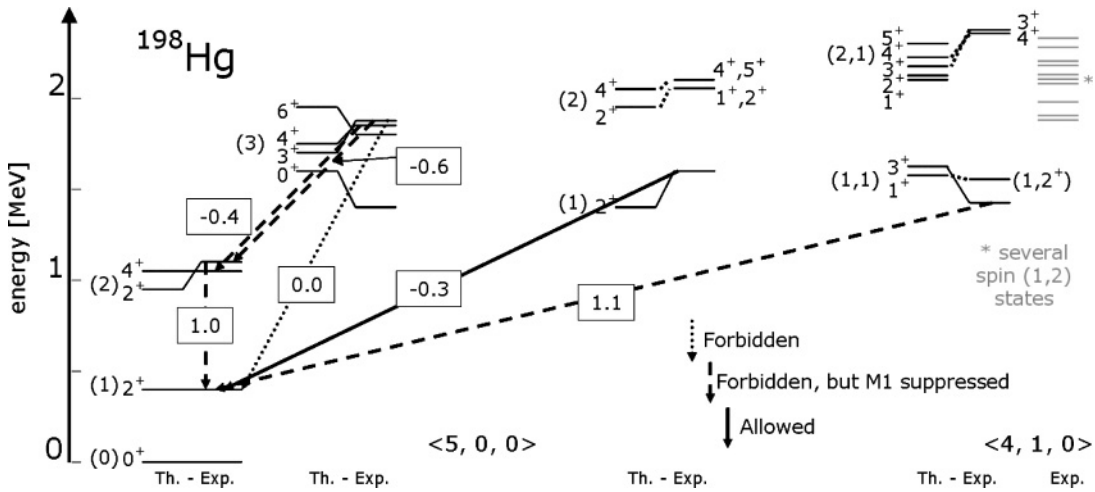

FIG. 5. Investigation of the $M1$ fraction of several γ transitions using the determined multipole mixing ratios δ. The transitions are tested with the derived $M1$ selection rules, Eq. (14), considering the relative $B(M1)/B(E2)$ fractions listed in Table II.

TABLE II. Relative fraction of the transition strength $B(M1)/B(E2)$ for the $(M1 + E2)$ transitions drawn as arrow in Fig. 5.

E_{Level} (keV)	E_γ (keV)	Multipole mixing ratio δ	$B(M1)/B(E2)$
1087.5	675.7	$0.95^{+0.23}_{-0.19}$	1.3×10^{-3}
1419.0	1007.4	$1.10^{+0.52}_{-0.34}$	2.3×10^{-3}
1612.2	1200.5	−0.25(14)	6.1×10^{-2}
1834.6	786.2	−0.39(23)	1.1×10^{-2}
1846.8	759.4	−0.56(16)	4.9×10^{-3}
	1435.1	+0.00(11)	∞

not necessarily break the $M1$ selection rules, since the $M1$ fraction can be strongly suppressed in comparison to the $E2$ fraction. This argument can be used for four γ transitions marked in Fig. 5 as $M1$ transitions between states breaking the selection rules for $M1$ transitions.

Table III shows calculated $B(E2)$ transition strengths and can be used for the investigation of $E2$ fractions, e.g., for the assignments of the spin 3^+ states at $E = 1419.0$ and 1846.8 keV. The calculated $B(E2; 3^+_2 \to 2^+_1)$ of the $\tau = (3)$ spin 3^+ state is 0, whereas the $B(E2)$ values for the transitions to the 2^+_2 and 4^+_1 states clearly differ from 0. This proportion rather matches the observed decay properties of the $E = 1846.8$ keV state than of the 3^+ state at $E = 1419.0$ keV. The calculated $B(E2)$ values in Table III show quite a good matching with the experimentally observed $B(E2)$ transition strengths [20], considering the simplicity of the used model. However, it has to be said that the strong $M1$ fraction of the $E_\gamma = 1435.1$ keV decay with $\delta(3^+ \to 2^+) = +0.00(11)$ conflicts with the $M1$ selection rules for both possible 3^+ assignments, indicating a slightly broken symmetry and a mixing of different states. Calculations with a small perturbation of

TABLE III. Comparison of existing experimental data [20] with numerically calculated $B(E2)$ values using $e = 0.18\ e$ b.

	$B(E2)$ (e^2 b^2)	
	Exp.	Calc.
$B(E2; 2^+_1 \to 0^+_1)$	0.197(1)	0.187
$B(E2; 4^+_1 \to 2^+_1)$	0.295(14)	0.237
$B(E2; 2^+_2 \to 0^+_1)$	0.002	0
$B(E2; 2^+_2 \to 2^+_1)$	0.062(10)	0.024
$B(E2; 3^+_1 \to 2^+_1)$	–	0.019
$B(E2; 3^+_1 \to 4^+_1)$	–	0
$B(E2; 3^+_1 \to 2^+_2)$	–	0
$B(E2; 4^+_2 \to 4^+_1)$	–	0.140
$B(E2; 4^+_2 \to 2^+_2)$	–	0.154
$B(E2; 3^+_2 \to 2^+_1)$	–	0
$B(E2; 3^+_2 \to 4^+_1)$	–	0.065
$B(E2; 3^+_2 \to 2^+_2)$	–	0.163
$B(E2; 6^+_1 \to 4^+_1)$	0.117(13)	0.228
$B(E2; 8^+_1 \to 6^+_1)$	0.082(41)	0.181

TABLE IV. Comparison of the new fit parameters of ^{198}Hg with the old fit parameters of the ^{196}Pt supermultiplet [4,13]. All parameters are given in MeV.

	A	B	C
^{198}Hg	−0.101	0.090	0.007
^{196}Pt	−0.097	0.042	0.025

the Hamiltonian by a quadrupole interaction with a strength of $\kappa(\tilde{Q} \cdot \tilde{Q}) = 10^{-4}$ reproduces these $M1$ transitions. It indicates a small rotor-like character of the nucleus ^{198}Hg. Note that this conforms with a prolate-oblate phase transition as has already been observed for the Hf-Hg mass region [24].

The level assignments matching both criteria best are shown in Figs. 5 and 6. For the chosen assignments, the resulting new parameters of a least-squares fit are $A = -0.101$, $B = 0.090$, and $C = 0.007$. A direct comparison of the new parameters and the parameters of the ^{196}Pt supermultiplet [4,13] is given in Table IV. One notices quite some changes in B and C giving the structure within a σ multiplet and a small change in A which determines the energy of the $\langle 4, 1, 0\rangle$ states. The difference in B causes a wider splitting for the τ multiplets, whereas the smaller parameter C reduces the splitting in J. This relation can be seen in energy equation (5). Because of the parameter relations of Eq. (6), this direct comparison is only possible for the even-even supermultiplet member ^{196}Pt.

Figure 6 compares the theoretical scheme with the experimentally determined level scheme. Experimental states that were used for fitting are connected to the theoretical predictions by lines. Figure 6 shows a good agreement with the theoretical states up to an energy of 2 MeV in ^{198}Hg.

While the $\langle 5, 0, 0\rangle$ part of the level scheme in Fig. 6 represents states from the sd IBA, additional states occur in the $\langle 4, 1, 0\rangle$ part. They are equivalent to the so-called mixed symmetry states [14]. For the $2^+_3 \to 2^+_1$ transition, a multipole mixing ratio of $\delta = -0.25(14)$ was determined, showing an important $M1$ contribution in agreement with expectations for mixed symmetry states.

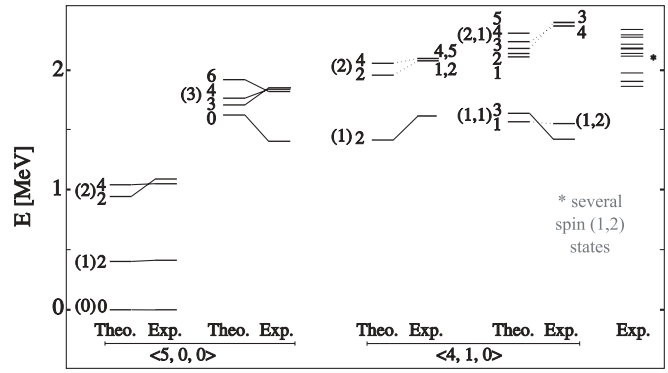

FIG. 6. Resulting fit for the adjusted new parameters. All states are labeled with their quantum numbers (τ_1, τ_2) and J and have positive parity.

VI. CONCLUSION

Within this work, we presented a theoretical approach expanding the four-member supermultiplet by a fifth two-fermions–N-bosons member, which should describe the even Hg isotopes, in particular ^{196}Hg and ^{198}Hg based on the supermultiplets around ^{194}Pt and ^{196}Pt.

Because of the shell structure in the Au-Pt mass region, considering $j_\pi = 3/2$ protons and the corresponding algebraic structure, this supermultiplet member can be described equivalently within the IBFFA and IBA-2 models in the case with no proton bosons. By showing the consistency of these two different models, we found a strong indication that configurations with more than one fermion do not necessarily always represent just higher excited broken pair states as described in Ref. [2], but can also form low-energy states present in IBA-2 applications.

To test the validity of the predictions for ^{198}Hg, a $\gamma\gamma$ angular correlation experiment was performed at the Tandem accelerator of the IKP Cologne, determining level spins and multipole mixing ratios to construct the low-energy level scheme of ^{198}Hg up to an excitation energy of 2.4 MeV. After a least-squares fit, the theoretical predictions match the experimental data quite well with fit parameters close to the ones describing the supermultiplet around ^{196}Pt [4,13]. We tested $M1$ transitions with derived $M1$ selection rules and calculated $B(E2)$ transition strengths within the extended supersymmetric model $\mathrm{U}_\nu(6/12) \otimes \mathrm{U}_\pi(6/4)$. The calculated $B(E2)$ values match the experimental data available [20] quite well considering the truncated model with only $j_\pi = 3/2$ protons.

In conclusion, it seems that the spectrum of ^{198}Hg—including the low-energy parts—can actually be related within the two-fermions–N-bosons description to the corresponding supermultiplet around ^{196}Pt.

ACKNOWLEDGMENT

This work was partially supported by Deutsche Forschungsgemeinschaft DFG under Grant Nos. Jo391/2-3 and Jo391/3-2.

[1] A. Arima and F. Iachello, *The Interacting Boson Model* (Cambridge University Press, Cambridge, England, 1987).
[2] F. Iachello and P. Van Isacker, *The Interacting Boson Fermion Model* (Cambridge University Press, Cambridge, England, 1991).
[3] F. Iachello, Phys. Rev. Lett. **44**, 772 (1980).
[4] P. Van Isacker, J. Jolie, K. Heyde, and A. Frank, Phys. Rev. Lett. **54**, 653 (1985).
[5] A. Metz, J. Jolie, G. Graw, R. Hertenberger, J. Gröger, C. Günther, N. Warr, and Y. Eisermann, Phys. Rev. Lett. **83**, 1542 (1999).
[6] J. Gröger *et al.*, Phys. Rev. C **62**, 064304 (2000).
[7] H.-F. Wirth *et al.*, Phys. Rev. C **70**, 014610 (2004).
[8] J. Jolie and P. E. Garrett, Nucl. Phys. **A596**, 234 (1996).
[9] M. Balodis *et al.*, Phys. Rev. C **77**, 064602 (2008).
[10] P. D. Duval and B. R. Barrett, Nucl. Phys. **A376**, 213 (1982).
[11] N. Blasi, S. Brandenburg, M. N. Harakeh, W. A. Sterrenburg, and S. Y. van der Werf, Phys. Rev. C **26**, 1893 (1982).
[12] P. Van Isacker, A. Frank, and H.-Z. Sun, Ann. Phys. (NY) **157**, 183 (1984).
[13] J. Jolie, Ph.D. thesis, University of Gent, 1986.
[14] P. Van Isacker, K. Heyde, J. Jolie, and A. Sevrin, Ann. Phys. (NY) **171**, 253 (1986).
[15] S. Heinze, Ph.D. thesis, University of Cologne, 2008.
[16] A. Linnemann, Ph.D. thesis, University of Cologne, 2005.
[17] I. Wiedenhöver, code CORLEONE, University of Cologne, 1995.
[18] K. S. Krane, R. M. Steffen, and R. M. Wheeler, At. Data Nucl. Data Tables **11**, 351 (1973).
[19] K. S. Krane and R. M. Steffen, Phys. Rev. C **2**, 724 (1970).
[20] Z. Chunmei, Nuclear Data Sheets **95**, 59 (2002).
[21] C. Bernards *et al.* (to be published).
[22] H. Klein, code TRANSNUCLEAR, University of Cologne, 2001.
[23] M. P. Fewell, Phys. Lett. **B167**, 6 (1986).
[24] J. Jolie and A. Linnemann, Phys. Rev. C **68**, 031301(R) (2003).